BNL-224823-2023-JAAM

GRP-COSC-4

Au/Pt Bimetallic Nanowires with Stepped Pt Sites for Enhanced C-C Cleavage in C2+ Alcohol Electro-oxidation Reactions

K. Wei, K. Sasaki

To be published in "Journal of the American Chemical Society"

August 2023

Chemistry Department

Brookhaven National Laboratory

U.S. Department of Energy

USDOE Office of Energy Efficiency and Renewable Energy (EERE), Fuel Cell Technologies Program (EE-3F)

DISCLAIMER

Au/Pt bimetallic nanowires with stepped Pt sites for enhanced C-C cleavage in C2+ alcohol electro-oxidation reactions

Kecheng Wei[1,†], Honghong Lin[1,†], Xueru Zhao[2,†], Zhonglong Zhao[3], Nebojsa Marinkovic[4], Michael Morales[1], Zhennan Huang[5], Laura Perlmutter[1], Huanqin Guan[1], Cooro Harris[1], Miaofang Chi[5], Gang Lu[6], Kotaro Sasaki[2]*, Shouheng Sun[1]*

AUTHOR ADDRESS

[1]Department of Chemistry, Brown University, Providence, Rhode Island 02912, United States

[2]Department of Chemistry, Brookhaven National Laboratory, Upton, New York 11973, United States

[3]School of Physical Science and Technology, Inner Mongolia University, Hohhot, China

[4]Department of Chemical Engineering, Columbia University, New York, NY 10027, United States

[5]Center for Nanophase Materials Sciences, Oak Ridge National Laboratory, Oak Ridge, Tennessee 37831, United States

[6]Department of Physics and Astronomy, California State University Northridge, Northridge, California 91330, United States

*Corresponding Author. Email: ssun@brown.edu, ksasaki@bnl.gov

†These authors contributed equally to this work.

KEYWORDS: Bimetallic nanowires, low-coordination surface, carbon-carbon bond cleavage, alcohol oxidation reaction, in situ spectroscopy, DFT calculations

ABSTRACT: Efficient C-C bond cleavage and oxidation of alcohols to CO_2 is key to developing highly efficient alcohol fuel cells for renewable energy applications. In this work, we report the synthesis of core/shell Au/Pt nanowires (NWs) with stepped Pt clusters deposited along the ultrathin (2.3 nm) stepped Au NWs as a robust catalyst to effectively oxidize alcohols to CO_2. The catalytic oxidation reaction is dependent on the Au/Pt ratios and the $Au_{1.0}/Pt_{0.2}$ NWs have the largest percentage (~75%) of stepped Au/Pt sites and show the highest activity for ethanol electrooxidation, reaching an unprecedented 196.9 A/mg_{Pt} (32.5 A/mg_{Pt+Au}). This NW catalyst is also active in catalyzing the oxidation of other primary alcohols, such as methanol, n-propanol, and ethylene glycol. In situ X-ray absorption spectroscopy and infrared spectroscopy are used to characterize the catalyst structure and to identify key reaction intermediates, providing concrete evidence that the synergy between the low-coordinated Pt sites and the stepped Au NWs is essential to catalyze the alcohol oxidation reaction, which is further supported by DFT calculations that the C-C bond cleavage is indeed enhanced on the under-coordinated Pt-Au surface. Our study provides a general design concept and synthesis of core/shell structure with stepped core/shell sites for enhanced electrochemical oxidation of alcohols, which will be central to the development of highly efficient direct alcohol fuel cells and other electro-oxidation reactions.

The difficulty in practical use of hydrogen to generate electricity has motivated the extensive search of alternative fuels for renewable energy applications. Ethanol is one of the most promising fuel candidates because it has almost eight times higher volumetric energy density than hydrogen (6.35 vs. 0.8 kWh/L, respectively) and can be massively produced from biomass. Although its oxidation reaction releases CO_2 inevitably, ethanol requires 23 times less processing energy than hydrogen (2.39 vs. 55 MWh/ton, respectively), which greatly reduces the life-cycle emission[1]. The oxidation of ethanol can be directly converted to electricity in fuel cells, also known as direct ethanol fuel cells (DEFCs), but the conversion efficiency is limited by the low activity of the state-of-the-art electrocatalysts in catalyzing ethanol oxidation reaction (EOR)[2].

The most common electrocatalysts studied for alcohol oxidation are Pt/Pd-based, and one of the major causes of the low EOR activity is the blockage of catalyst surface sites by various reaction intermediates[3]. Although the detailed mechanism leading to EOR remains unclear due to the complexity of the multiple electron/proton transfer processes, it is generally agreed that the oxidation follows two possible pathways: (a) the C1 pathway that delivers twelve electrons, which involves C-C cleavage and conversion of the resulting C1 intermediates (CO*, CH_x*, etc) to CO_2; and (b) the C2 pathway that transfers four electrons and/or two electrons to form acetic acid and/or acetaldehyde[3]. In both pathways, various reaction intermediates can strongly bind to the catalyst surface, blocking the catalyst active sites, and removal of these intermediates requires the participation of another oxygenated intermediate, OH*, which is difficult to form on the Pt/Pd surface[4,5]. To facilitate OH*

formation, the EOR is often tested in alkaline media in the presence of an alloy catalyst (e.g. Pt-Ag, Pt-Au)[6–9] or the Pt/Pd catalyst alloyed with another oxophilic transition metal component[10–13]. Despite these efforts, the activity enhancement often originates from the accelerated C2 pathway with acetate and acetaldehyde being detected as the predominant EOR products, as characterized by infrared spectroscopy[11,15,16], differential electrochemical mass spectrometry[16], and nuclear magnetic resonance[17].

In 2009, Adzic's group found that a synergistic effect of the ternary system Pt-Rh-SnO_2, where Pt adsorbs ethanol, SnO_2 adsorbs OH*, and Rh splits C–C bond, could facilitate C-C cleavage and the overall EOR activity[11]. The similar synergistic effect was observed in other multi-component systems, such as Pt-Ir-SnO_2[18], Au-Pt-Ir[19], and Cu-Pd-Ir[20]. A record-high EOR activity was achieved on the Au/Pt-Ir core/shell catalyst in alkaline media with its mass activity reaching 58 A/mg_{Pt+Ir} and the C1 selectivity of 57%. Surface defect control is another way of increasing the EOR activity. Low-coordinated surfaces were found to split the C-C bond more effectively than closed-pack Pt(111)[21,22,23]. However, this factor is limited to the EOR activity enhancement possibly due to the competition between surface poisoning and C-C cleavage[24]. Therefore, to achieve a high EOR activity with good C1 pathway selectivity, both poisoning intermediate removal and C-C cleavage improvement need to be considered.

In this study, we combine the composition and surface morphology control to simultaneously address the poisoning and C-C cleavage issues in the EOR. Since Au-Pt bimetallic system has shown exceptional anti-poisoning effect against CO*-intermediates in formic acid oxidation[25] and methanol oxidation reaction[26], we construct low-coordinated facets composed of Pt and Au clusters along the Au/Pt nanowire (NW) structure. Using a seed-mediated growth method, we synthesized ultrathin (2∼3 nm) core/shell Au/Pt NWs, with abundant low-coordinated Au-Pt sites exposed on the catalyst's surface. This core/shell Au/Pt NW catalyst shows exceptionally high EOR activity in alkaline media, achieving peak activity of 196.9 A/mg_{Pt} (32.5 A/mg_{Pt+Au}). The enhanced catalytic activity can be extended to oxidize other primary alcohols, such as methanol, n-propanol, and ethylene glycol. The key intermediate steps related to OH* adsorption and C-C cleavage are confirmed by in situ X-ray absorption spectroscopy (XAS) and IR, providing concrete evidence on using the Au/Pt NW structure to solve the CO* poisoning and OH* adsorption issues that are key to enhancing C1-pathway selectivity and improving catalytic efficiency of the EOR. Density functional theory (DFT) calculations reveal that the low-coordinated AuPt surface (for example, the model AuPt(211) or AuPt(221) surface) indeed lowers the energy barriers for C-C bond cleavage and CO* activation/desorption, more efficiently catalyzing the oxidation of alcohols to CO_2.

Results and Discussion

Catalyst synthesis and characterization. Ultrathin 2.3 nm Au NWs (**Fig. 1A, Fig. S2**) were prepared by reduction of $HAuCl_4$ precursor in an oleylamine (OAm) and hexane micelle solution as reported[27]. The micelle serves as a soft template and facilitates the NW morphology formation. Pt was deposited onto the ultrathin Au NWs by the reduction of $Pt(acac)_2$ in an OAm solution with *tert*-butylamine borane (TBAB) as a reducing agent at 140 ˚C. The amount of Pt deposition was controlled by the amount of Pt precursor and TBAB, and three different compositions were synthesized in this work and confirmed with ICP: $Au_{1.0}/Pt_{0.2}$ NWs, $Au_{1.0}/Pt_{0.5}$ NWs, and $Au_{1.0}/Pt_{1.0}$ NWs. The as-synthesized Au/Pt NWs are about 2 - 3 nm in diameter and μm-range in length (**Fig. 1B, Fig. S1, 2**). In the same synthetic condition without adding the Pt precursor and TBAB, smooth Au NWs would degrade first into zig-zag shaped NWs, and finally to spherical nanoparticles (**Fig. S3A**). If the reaction temperature was set too high (160 ˚C), Pt would self-nucleate into nanoparticles rather than grow on Au NWs (**Fig. S3B**). Thus, the deposition of Pt onto Au NWs is successfully controlled through the reduction of $Pt(acac)_2$ in the presence of TBAB at 140 ˚C. In this Pt deposition condition, the zig-zag Au NWs initially formed were more efficiently stabilized by the deposited Pt without further degrading into Au nanoparticles. HAADF-STEM and elemental mapping images reveal the core/shell Au/Pt structure (**Fig. 1 C-G, Fig. S1 C-G**). The average thickness of the Pt coating over the Au NWs is 0.3 nm for $Au_{1.0}/Pt_{0.2}$ NWs and 0.6 nm for $Au_{1.0}/Pt_{1.0.}$ NWs. The Pt coating layers are populated with low-coordinated Pt on the surface. The as-synthesized Au/Pt NWs still maintain the face centered cubic (fcc) structure (**Fig. S4**). Lattice fringes of the deposited Pt are 0.233 nm for (111) and 0.203 nm for (200), both larger than those of pure Pt (0.227 nm and 0.196 nm respectively) (**Fig. 1C**), indicating that the Pt-Pt bond in the deposited Pt is stretched due to the epitaxial growth of Pt on Au NWs.

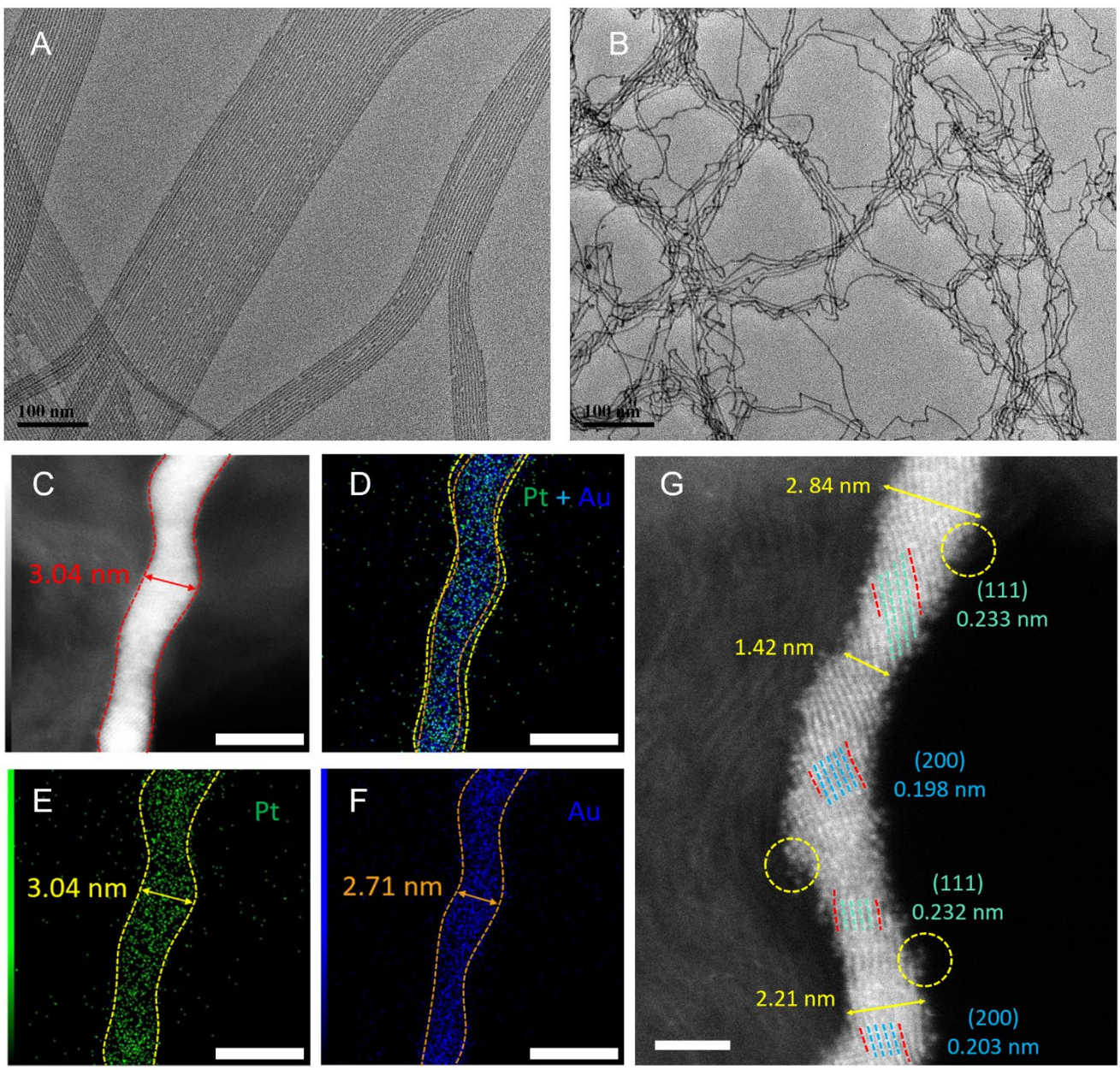

Figure 1. TEM images of (**A**) Au NWs, (**B**) $Au_{1.0}/Pt_{0.2}$ NWs. (**C-F**) High-angle annular dark-field scanning transmission electron microscopy (HAADF-STEM) image and two-dimensional mapping of Pt-Lα (green) and Au-Lα (blue) energy-dispersive spectroscopy (EDS) intensities for a typical $Au_{1.0}/Pt_{0.2}$ NW. Scale bar: 5 nm. (**G**) High-angle annular dark-field scanning transmission electron microscopy (HAADF-STEM) image of an $Au_{1.0}/Pt_{0.2}$ NW. Scale bar: 2 nm.

The core/shell structure was further analyzed by cyclic voltammetry (CV) to obtain surface Au/Pt ratios based on the reduction peak areas of the electro-oxidized Au and Pt (**Fig. S5A-B**). The Au:Pt ratios of three different Au/Pt NWs were calculated to be 1:2.6, 1:0.72, and 1:0.54 for $Au_{1.0}/Pt_{1.0}$ NWs, $Au_{1.0}/Pt_{0.5}$ NWs, and $Au_{1.0}/Pt_{0.2}$ NWs, respectively. Compared to the bulk compositions analyzed by ICP, the reduction peaks show the higher Pt ratios, suggesting the accumulation of Pt on the Au surface. An increase in the potential of the Pt reduction peak with a decrease in Au/Pt ratio was observed in the CV curves (**Fig. S5B**). The positive shifts indicate the electronic interaction between the surface Pt and sublayer Au, which is also seen in XPS spectra (**Fig. S5C-D**). An obvious negative shift of Pt 4f scan is observed in Au/Pt samples, and the effect is stronger when less Pt is presented on the Au surface. Contrary to the case of surface Pt, no discernible shift in Au 4f scans is observed since the most Au stays in the core with no interaction with the surface Pt.

CO is a typical intermediate formed in the ethanol oxidation process and is known to deactivate Pt-based catalyst due to the strong Pt-CO interaction. We examined the CO poisoning effect on our Au/Pt NWs by studying CO oxidation reaction in the presence of NWs (**Fig. S6**). On Au NWs and $Au_{1.0}/Pt_{0.2}$ NWs, an oxidation peak around 0.4 V was observed, which is comparable to the previously reported CO oxidation peak on Au in alkaline media[28]. On $Au_{1.0}/Pt_{0.5}$ NWs and $Au_{1.0}/Pt_{1.0}$ NWs, two

oxidation peaks at 0.5 V and 0.8 V show up, which indicates two types of CO adsorption sites on the NW surfaces. This split oxidation behavior is likely caused by the presence of segregated Pt clusters on the Au surface as Pt content increases. The segregated Pt binds with CO more strongly than that on Au-Pt sites. The CO oxidation profiles of all three kinds of Au/Pt NWs indicate the obvious Au substrate effect on promoting CO desorption.

Electrochemical EOR. To study the ethanol oxidation catalysis of Au/Pt NWs, the catalyst was first subject to 30 cycles of CV scans between 0 and 1.0 V at 100 mV/s in 1 M KOH solution at room temperature to obtain a stable CV curve. CV in 1 M KOH + 1 M ethanol solution was then performed to study the catalytic oxidation of ethanol. Au NWs showed no detectable activity towards the EOR from 0 to 1.2 V, while commercial Pt/C exhibited a peak current density of 0.98 A/mg_{Pt} for the EOR at 0.75 V (**Fig. S7**). CVs for the EOR of the Au/Pt NW catalysts are presented in **Fig. 2A**. The mass activity increases with the decrease of the Pt amount in the Au/Pt structure (**Fig. 2B**). Such a trend also coincides with the 1st and 2nd CO oxidation peak ratio (**Fig. S6**), suggesting a correlation between the efficiency of intermediates removal and the high EOR activity. Among these three Au/Pt NWs, $Au_{1.0}/Pt_{0.2}$ NWs show the highest oxidation peak at 0.9 V with the mass activity being calculated to be 196.9 A/mg_{Pt} (32.5 A/mg_{Pt+Au}), which is about 190 times higher than the commercial Pt (0.98 A/mg_{Pt}) (**Fig. 2B**). To the best of our knowledge, this is the highest mass activity for the EOR reported in literature (**Fig. S8**). Furthermore, these Au/Pt NWs were found to be active in oxidation of not only ethanol, but other alcohols as well (**Fig. 2C-D**). The observed increase in mass activity from the oxidation of methanol, ethanol, n-propanol and ethylene glycol indicates that the catalyst is especially active in cleaving C-C bond and catalyzing the oxidation of primary alcohols. However, the catalyst has limited activity towards the oxidation of secondary alcohol (isopropanol we tested in this paper) (**Fig. 2D**).

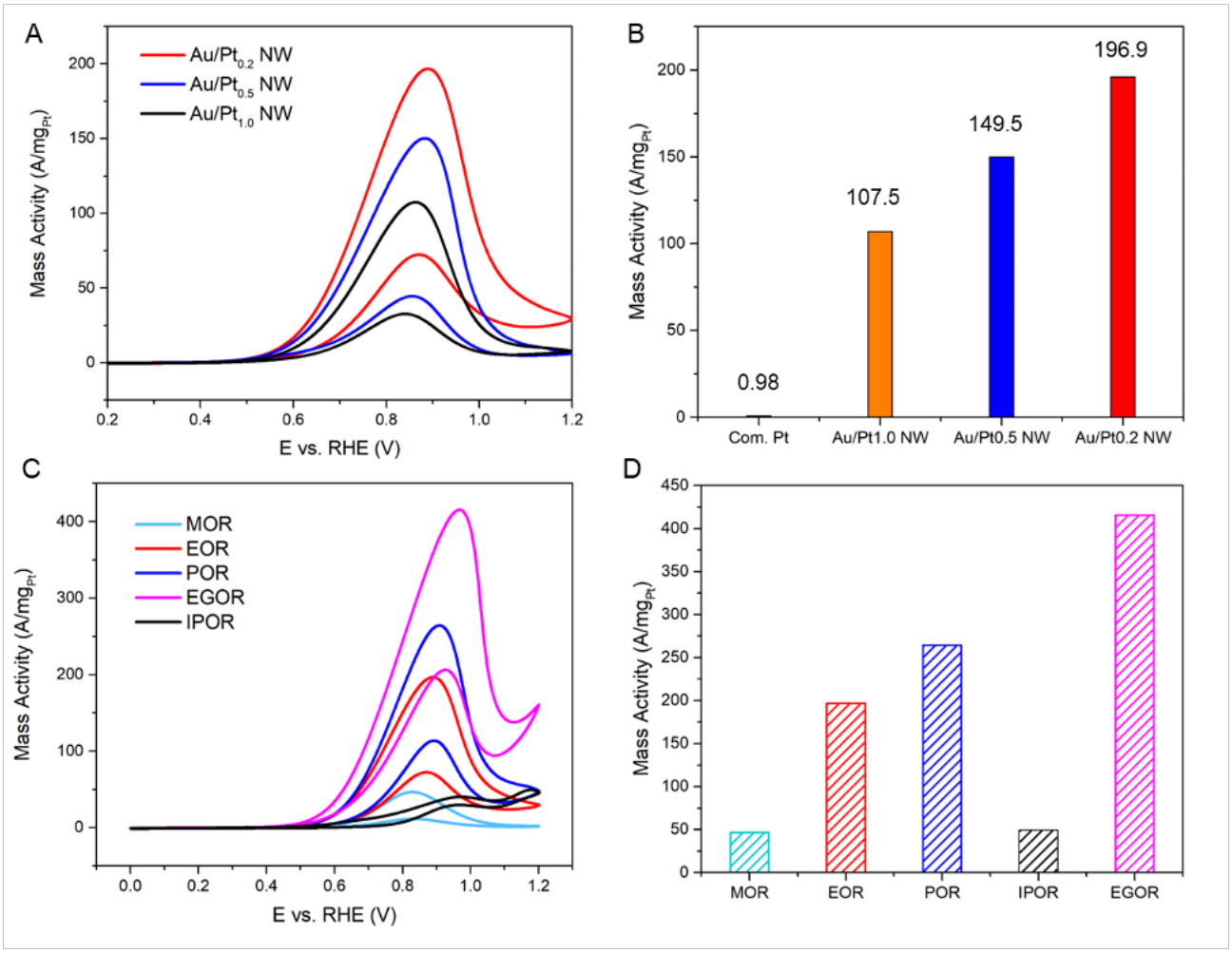

Figure 2. (**A**) Ethanol oxidation cyclic voltammetry of $Au_{1.0}/Pt_{0.2}$ NWs, $Au_{1.0}/Pt_{0.5}$ NWs and $Au_{1.0}/Pt_{1.0}$ NWs. (**B**) Mass activity of $Au_{1.0}/Pt_{0.2}$ NWs, $Au_{1.0}/Pt_{0.5}$ NWs and $Au_{1.0}/Pt_{1.0}$ NWs and commercial Pt in 1 M KOH and 1 M ethanol solution. (**C**) Cyclic voltammetry curves of $Au_{1.0}/Pt_{0.2}$ NWs in 1 M KOH + 1 M alcohol. MOR: methanol, EOR: ethanol, POR: propanol, EGOR: ethylene glycol, IPOR: isopropanol oxidation reactions, and the corresponding peak mass activity (**D**).

Electrochemical Operando XAS. To gain more insights of the EOR enhancement on the Au/Pt NW catalyst, we first studied changes in atomic structure and electronic state of the catalyst during the EOR via in situ X-ray absorption near-edge structure (XANES) techniques[29]. The Pt L_3-edge XANES spectra of the $Au_{1.0}/Pt_{0.2}$ NW catalyst were obtained in a potential region from 0.4 to 1.1 V in 1 M KOH and 1 M KOH + 1 M ethanol solutions, as shown in **Fig. 3A-B**. In the 1 M KOH solution, upon increasing

the potential, the intensity of the white line of Pt L_3-edge increases and its adsorption peak is shifted to higher energies as a consequence of the depletion of Pt's d-band due to the formation of Pt oxides. In contrast, in the 1 M KOH + 1 M ethanol solution, the $Au_{1.0}/Pt_{0.2}$ NW catalyst shows no obvious changes in white line intensity with increasing potentials. The potential dependence of Pt oxidation in the two solutions is more clearly presented in **Fig. 3C**, which shows changes in the white line intensity (ΔWL) relative to that at a double layer region (0.4 V) ((ΔWL(*E*) –ΔWL(0.4V)/ΔWL(0.4V)) as a function of the applied potentials. The white line intensity of the $Au_{1.0}/Pt_{0.2}$ NWs increases with increasing potentials in 1 M KOH due to the formation of PtOH or PtO_2, while no sign of Pt oxidation is observed until 0.9 V with a small rise at 1.1 V in 1 M KOH + 1 M ethanol. The result suggests that the oxidization of ethanol is the main anodic reaction for the $Au/Pt_{0.2}$ NW catalyst in the ethanol-containing solution and the formation of Pt oxides on the catalyst surface is significantly suppressed. A similar observation was seen for commercial Pt/C as shown in **Fig. S9**, although the following detailed analysis reveals that the surface of $Au_{1.0}/Pt_{0.2}$ NWs behaves quite differently from that of Pt/C. The XAS data obtained were further analyzed by the $\Delta\mu$ method[30–33], which has been developed as a surface-sensitive method to identify surface/adsorbate interactions. By subtracting spectra of a sample at two different potentials, the $\Delta\mu$ method isolates surface/adsorbate interactions because bulk metal-metal interactions are nearly eliminated by the subtraction. **Fig. 3D-F** show $\Delta\mu$ spectra of the commercial Pt/C and $Au_{1.0}/Pt_{0.2}$ NW catalyst in 1 M KOH, calculated by the equation ($\Delta\mu(E, \text{KOH}) = \mu(E, \text{KOH}) - \mu(0.4\text{V}, \text{KOH})$), which show positive peaks at 11568 eV, 4 eV above the edge energy E_0 (11564 eV for Pt L_3 edge) (indicated by a circle in **Fig. 3D**). The observation is interpreted as the initiation of O or OH adsorption in atop sites of Pt atoms[30–33]. Another but more interesting feature of the Pt/C is that a negative peak slightly below the E_0, starts to further decrease ≥ 0.9 V, which is attributed to the formation of subsurface O due to the "place-exchange" process, as indicated by comparison to the theoretically calculated $\Delta\mu$ spectral signatures[32,33]. In contrast, the $Au_{1.0}/Pt_{0.2}$ NWs do not show such a change at ≥ 0.9 V (indicated by a circle in **Fig. 3D**). Both the commercial Pt and $Au_{1.0}/Pt_{0.2}$ show an increase of O or OH adsorption in atop sites of Pt at more positive potentials, but their behavior differs for subsurface oxygen. A stronger signal from subsurface O due to the "place-exchange" can be observed from the commercial Pt at higher potentials, while no detectable changes are observed from the $Au_{1.0}/Pt_{0.2}$ NWs because its surface Pt structure is a sub-monolayer and these Pt atoms are stabilized by the subsurface Au. **Fig. 3F** shows another $\Delta\mu$ spectra of $Au/Pt_{0.2}$ NWs, which were calculated by the equation ($\Delta\mu(E, \text{EtOH}) = \mu(E, \text{EtOH}) - \mu(0.4\text{V}, \text{KOH})$), to examine the effect of ethanol/intermediates adsorption in 1 M KOH + 1 M EtOH at different potentials relative to that at 0.4 V in 1 M KOH. By subtracting the spectrum at 0.4 V in 1 M KOH from that of 1 M KOH + 1 M ethanol, the $\Delta\mu$ method can retrieve only the catalyst surface interaction with the adsorbates, i.e., reactants and intermediates during the EOR. The feature of $\Delta\mu$(0.4 V, EtOH) for $Au/Pt_{0.2}$ NWs comprising a negative peak at 11565 eV coupled with a positive peak at 11570 eV is similar to that of $\Delta\mu$ spectra of Pt/C obtained in an ethanol-containing solution in open circuit by subtracting the measurement for water at 0.45 V[30]. The $\Delta\mu$ spectra of $Au_{1.0}/Pt_{0.2}$ NWs remain almost steady at potentials from 0.4 V to 1.1 V, suggesting that a reaction mechanism for the EOR is unchanged. Contrary to that, the intensity in $\Delta\mu(E, \text{EtOH})$ spectra of the commercial Pt shows an obvious potential dependency (**Fig. S10**), indicating the change of reaction mechanisms on Pt with applied potentials, which has been discussed in previous works[3,21]. We note that the L_3-edge adsorption edges of Pt (11564 eV) and Au (11919 eV) are very close (only 355 eV apart), which makes it impossible to fit Pt L_3 and Au L_3 signals of the Au/Pt NW catalyst to examine the detailed atomic structures from the extended X-ray absorption fine structure (EXAFS) analysis.

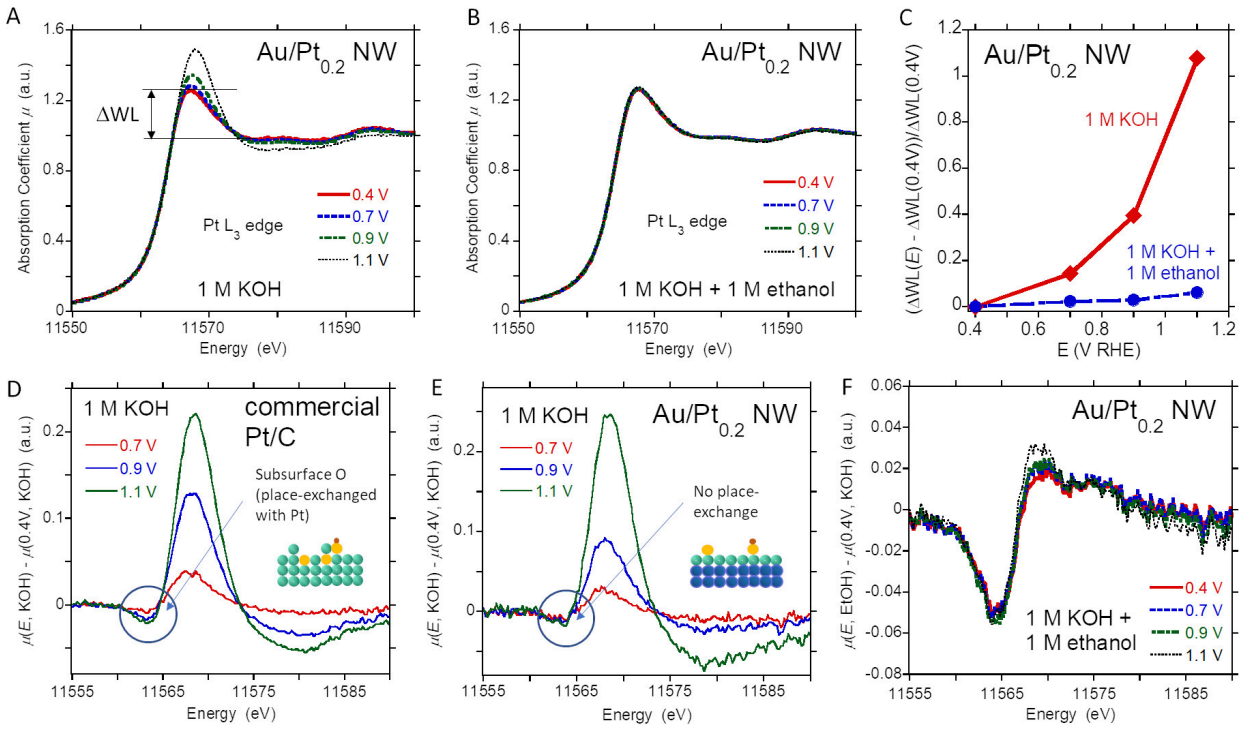

Figure 3. In situ Pt L_3-edge XANES of $Au_{1.0}/Pt_{0.2}$ NW catalyst at different potentials in 1 M KOH (**A**) and 1 M KOH + 1 M ethanol (**B**). (**C**) Comparison of relative changes in white line intensity ((ΔWL(*E*) – ΔWL(0.4V)/ ΔWL(0.4V) of $Au_{1.0}/Pt_{0.2}$ NW catalyst in the two solutions, plotted as a function of applied potentials. Pt L_3-edge Δμ spectra (Δμ(*E*, KOH) = μ(*E*, KOH) - μ(0.4V, KOH), where E = 0.7, 0.9, and 1.1 V)) of commercial Pt/C (**D**) and $Au_{1.0}/Pt_{0.2}$ NW catalyst (E) in a 1 M KOH solution. (**F**) Pt L_3-edge Δμ spectra ((Δμ(*E*, EtOH) = μ(*E*, EtOH) - μ(0.4V, KOH), where *E* = 0.4, 0.7, 0.9, and 1.1 V)) of $Au_{1.0}/Pt_{0.2}$ NW catalyst (EtOH = 1 M KOH + 1 M ethanol).

In situ IRRAS measurements. In situ IRRAS experiments were performed to identify the intermediates and products and understand the selectivity of C-C cleavage during the EOR. The absorbance spectra given in **Fig. 4** show the behavior of adsorbance on Pt/C, $Au_{1.0}/Pt_{0.2}$ NWs, and $Au_{1.0}/Pt_{0.5}$ NWs in 1 M KOH and 1 M ethanol, where the positive- and negative-going peaks represent the gain and loss of species at the sample potential. **Supporting Table 1** lists the IR frequencies and their assignments. On the commercial Pt/C, ethanol oxidation begins from low potentials (>0.38 V), evidenced by the increasing of current density and the negative-going features at ~1040 & 870 cm^{-1}, representing the loss of ethanol in the solution (**Fig. 4A)**. Simultaneously with the loss of ethanol, positive-going peaks representing the gain of acetaldehyde (CH_3CHO) (1620~1635, 933 cm^{-1}), and acetate (CH_3COO^-) (1400, 1350 cm^{-1}) adsorbed on the Pt surface emerge. The intensity of these peaks stays practically constant until potential reaches 0.9 V. With the further increase in potential beyond 0.9 V, the intensity of the adsorbed CH_3CHO & CH_3COO^- peaks decreases, while two new peaks emerge at 1280 and 1700 cm^{-1}. These new peaks correspond to CH_3COO^- & CH_3CHO in the solution, indicating a partial desorption of CH_3COO^-* and CH_3CHO*. Partial oxidation of CH_3COO^-* and CH_3CHO* is observed above 0.88 V as indicated by the emergence of CO_2 peak at 2343 cm^{-1}. Because the initially generated CO_2 could react with OH^- to form CO_3^{2-} that shows a single band ~1390 cm^{-1} and would be totally covered by the acetate peaks (CH_3COO^-) (1400, 1350 cm^{-1}), the CO_2 peak at 2343 cm^{-1} would notbe observed until the CO_2 became neutralized in the thin layer of KOH electrolyte[34]. Based on the analysis above, on the pure Pt surface, ethanol is oxidized into acetaldehyde and then acetate, most of which are released into the solution from catalyst surface before they are further oxidized to CO_2. On the $Au_{1.0}/Pt_{0.2}$ surface (**Fig. 4B**), the adsorbed [CH_3COO^-]* & [CH_3CHO]* (1620~1635, 933 cm^{-1}, and 1400, 1350 cm^{-1}) were also detected starting from low potentials (>0.37 V), however, no peaks for the CH_3COO^- & CH_3CHO in the solution were detected, indicating that [CH_3COO^-]* & [CH_3CHO]* stay adsorbed on the catalyst surface and are further oxidized to CO_2, evidenced by the positive-going CO_2 peak above 0.97 V. Because $Au_{1.0}/Pt_{0.2}$ NWs have a smaller total Pt amount than Pt/C, the accumulated CO_2 amount might be too low to be detected by IR when C-C cleavage initially occurs, by resulting in a higher onset potential of CO_2 peak appearance (0.97 V vs. 0.88 V). For the similar reason, the accumulated CO_2 peak was not observed until 0.97 V on $Au_{1.0}/Pt_{0.5}$ and $Au_{1.0}/Pt_{1.0}$ NWs (**Fig. 4C**, **Fig. S11**). However, the desorbed CH_3COO^- & CH_3CHO in the solution were detected on $Au_{1.0}/Pt_{0.5}$ and $Au_{1.0}/Pt_{1.0}$ NWs, indicating their inferior C-C cleavage selectivity compared to $Au_{1.0}/Pt_{0.2}$ NWs. To compensate the difference of the accumulated CO_2 induced by the Pt loading, we normalized the CO_2 peak intensity at 1.1 V by each Pt mass as shown in **Fig. 4D**, where the $Au_{1.0}/Pt_{0.2}$ NW catalyst shows the highest C1 selectivity, about 3 times higher than that of Pt/C.

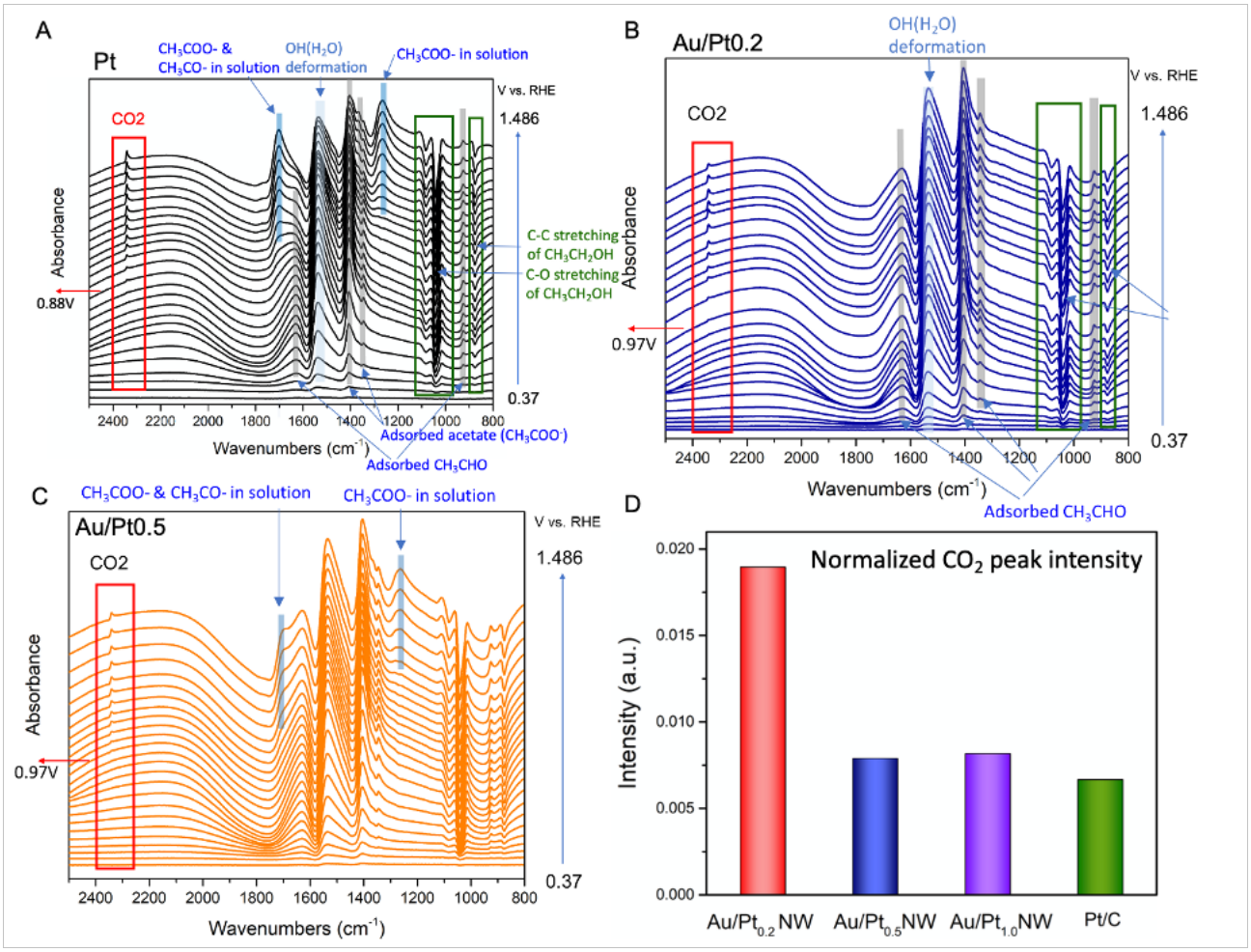

Figure 4. In situ IRRAS spectra of Pt/C (**A**), $Au_{1.0}/Pt_{0.2}$ NWs (**B**), and $Au_{1.0}/Pt_{0.5}$ NWs (**C**) as a function of potential from 0.37 V to 1.486 V (vs. RHE) in 1 M KOH + 1 M ethanol electrolyte. (**D**) Intensity of CO_2 peaks at 1.1 V normalized by each Pt mass.

Proposed EOR mechanism. The under-coordinated Pt and Au sites along the $Au_{1.0}/Pt_{0.2}$ NW surface must act synergistically to enhance its catalysis for the EOR enhancement. Strain in surface atoms induced by substrate materials alters the position of the d-band center of the surface atoms, resulting in changes in surface reactivity, according to the d-band theory of Norskov and co-workers[35,36]. The Au sites help to enhance the adsorption of reactants and intermediates on the Pt sites through substrate-induced lateral strain in Pt. The Au-Au bond is longer than the Pt-Pt bond, thereby the epitaxial growth of Pt over Au leads to the Pt-Pt expansion, as shown in the high-resolution microscopy analysis (**Fig. 1G**). This expansion upshifts the d-band center of Pt and induces the stronger adsorption of ethanol molecules and OH^- species, accelerating the partial oxidation of ethanol (reaction [1])[37], in which the intermediates of $[CH_3CHO]^*$ and $[CH_3COO^-]^*$ generated are strongly adsorbed on the Pt surface and are not easily released to the solution, as demonstrated in **Fig. 4B**. As shown in the $\Delta\mu$ spectra in the ethanol-containing solution (**Fig. 3F**), this oxidation process remains nearly intact up to 1.1 V. Since no "place-exchange" process occurs on the $Au_{1.0}/Pt_{0.2}$ NW catalyst (**Fig. 3E**), the surface Pt structure of the catalyst is stable up to the high potential. Therefore, the high EOR activity of the $Au_{1.0}/Pt_{0.2}$ NW catalyst is partly ascribed to fast kinetics of partial oxidation (reaction [1]) to $[CH_3CHO]^*$ and $[CH_3COO^-]^*$ on the stable and stretched Pt surface. The IRRAS measurements show that the EOR catalyzed by $Au_{1.0}/Pt_{0.5}$ or $Au_{1.0}/Pt_{1.0}$ NWs tend to yield more free CH_3CHO and CH_3COO^- in the solution due to the weak adsorption of $[CH_3CHO]^*$ and $[CH_3COO^-]^*$ on the thicker Pt surface that has a near normal Pt-Pt distance.

$$CH_3CH_2OH \rightarrow [CH_3CH_2OH]^* \rightarrow [CH_3CHO]^*/[CH_3COO^-]^* \rightarrow CH_3CHO/CH_3COO^- \quad [1]$$

$$CH_3CH_2OH \rightarrow [CH_3CH_2OH]^* \rightarrow [CH_3CHO]^*/[CH_3COO]^*/[CH_xCO]^* \rightarrow CO^* \rightarrow CO_2 \quad [2]$$

The enhanced EOR can also be attributed to the presence of stepped Au/Pt sites along the $Au_{1.0}/Pt_{0.2}$ NW surface. Feliu *et al*. have found that oxidation of ethanol on Pt[n(111) × (110)]-type electrodes takes place on the step sites, yielding CO_2 as the major final product, since the steps catalyze the cleavage of the C-C bond and also oxidation of the adsorbed CO species[38,39]. We consider that the stepped Pt sites along the stepped Au NW surface promote the cleavage of C-C bonds in $[CH_3CHO]^*/[CH_3COO^-]^*/[CH_xCO]^*$ to CO*, and then further oxidation of CO* to CO_2 (reaction [2]). To verify our hypothesis, we compare the activation energy of C-C bond cleavage and the free energy change of CO* desorption on different surfaces by density functional theory (DFT) calculations (**Fig. 5A, B**). We use AuPt(211) [= 2(111) × (100)] and AuPt(221) [= 2(111) ×

(110)] to represent the stepped surfaces with Au and Pt atoms, which two stepped surfaces have the highest step density of all [n(111) × (hkl)] planes. As shown in **Fig. 5A**, pure Au surfaces (i.e., Au(111), Au(100), Au(211), Au(221)) are not favorable for C-C cleavage. In previous in situ IRRAS study, there was also no clear sign of CO* and CO_2 generation on Au(111)/Pt_{ML} during the EOR[37], suggesting that Au substrate does not contribute to the C-C bond cleavage by itself. On stepped Pt(211), C-C cleavage can occur more facile than Pt(111), but the CO* desorption is impeded. The addition of Pt to the stepped Au surfaces (i.e., AuPt(211) and AuPt(221)) lowers the energy barrier for C-C bond cleavage as well as the CO* desorption, and the CO* desorption energy barrier is even lower in presence of surface oxidants (O*). The OH^- that strongly adsorbed on the stretched Pt surface likely helps the oxidation of CO*. We thus conclude that the considerable enhancement of the catalytic EOR activity of the $Au_{1.0}/Pt_{0.2}$ NWs is achieved by the synergy between the surface stepped and stretched Pt on the stepped Au NW substrates. The stepped Pt sites are also present on the $Au_{1.0}/Pt_{0.5}$ and $Au_{1.0}/Pt_{1.0}$ NWs, but thicker Pt deposition on the Au NW structure reduces the stepped Pt sites and releases the stretching degree of the Pt-Pt bond, facilitating the desorption of [CH_3CHO]* and [CH_3COO^-]* before their C-C bonds are cleaved (**Fig. 5C**), lowering their EOR catalytic activity, which is evidenced by the lower CO_2 intensity observed on Pt-rich surfaces (**Fig. 4D**).

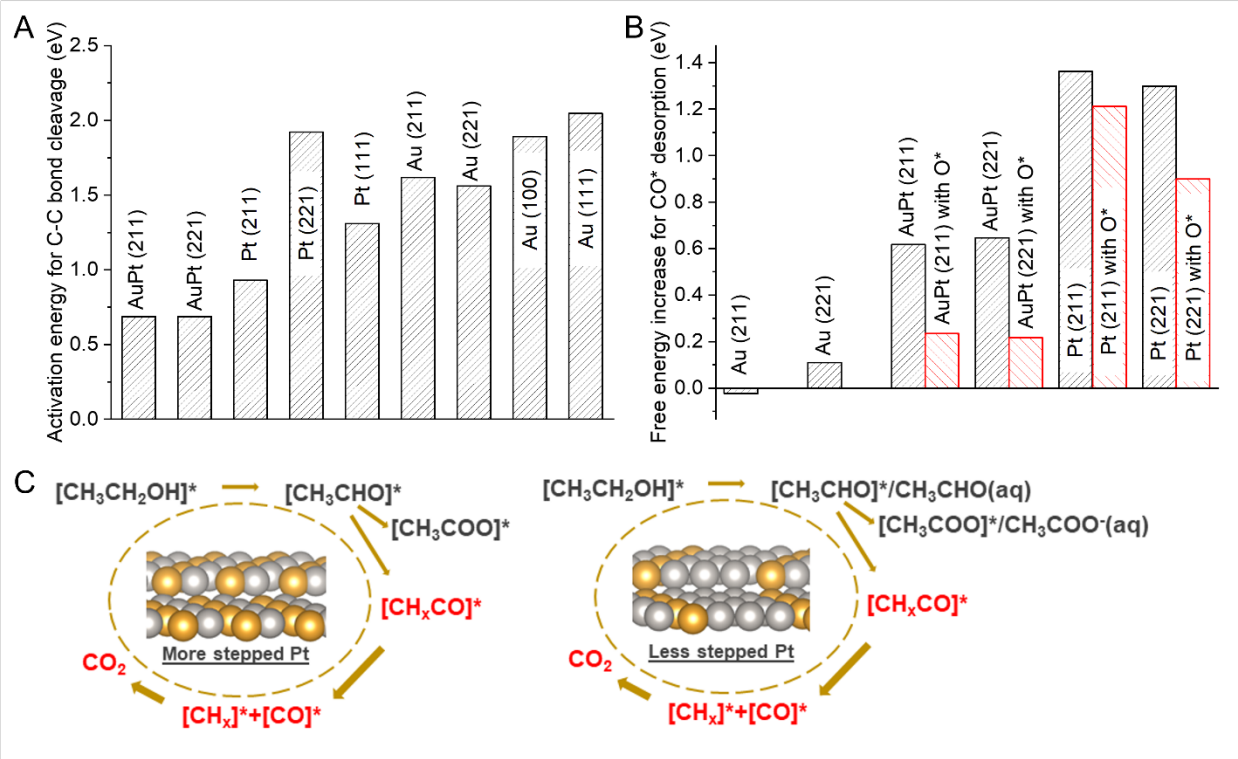

Figure 5. DFT calculations on (**A**) relative energy of C-C bond cleavage on AuPt(211), AuPt(221), Pt(211), Pt(221), Pt(111), Au(211), Au(221), Au(100), and Au(111) facets (**B**) free energy increase for CO* desorption on Au(211), Au(221), AuPt(211), AuPt(221), Pt(211), Pt(221) with/without oxidants, and (**C**) Schematic illustration of the C-C cleavage mechanism on stepped Au-Pt(221) surfaces with more stepped Pt (left) and less stepped Pt sites (right).

Conclusion

The present study has shown that the low-coordinated Pt sites in conjunction with the stepped Au is critical for enhancing electrochemical oxidation of ethanol. Using the ultrathin (2.3 nm) Au NWs as a template, we developed a reliable solution phase process to deposit Pt along the Au NWs, forming a unique core/shell-type Au/Pt structure with stepped Pt clusters exposed along the stepped Au NWs. These Au/Pt NWs show no sign of morphology change in the solution phase processes and are much more robust than the template Au NWs that tend to undergo morphology ripening to form spherical nanoparticles. Among three different Au/Pt NWs prepared and studied in this work, the $Au_{1.0}/Pt_{0.2}$ NWs provide the highest percentage (~75%) of bimetallic Pt-Au stepped sites and are most active for catalyzing EOR in alkaline media with mass activity reaching an unprecedented 196.9 A/mg_{Pt}. This enhanced catalysis is attributed to the desired synergy between the stepped Au and Pt sites, which promotes C-C cleavage, weakens the CO adsorption, and improves the OH adsorption, as characterized by in situ X-ray absorption spectroscopy, the $\Delta\mu$ method analysis, in situ IR, and DFT calculations. As a result, our $Au_{1.0}/Pt_{0.2}$ NW catalyst has the highest C1 selectivity ever reported towards full oxidation of ethanol to CO_2. Furthermore, the enhanced catalytic oxidation capability of the structure has been extended to electro-oxidize methanol, n-propanol, and even ethylene glycol. In all, our study provides a general design concept and synthesis of core/shell structure with stepped core/shell sites for enhanced electrochemical oxidation of alcohols, which will be central to the development of highly efficient direct alcohol fuel cells and other electro-oxidation reactions.

ASSOCIATED CONTENT

Supporting Information. **Figure S1-11** and **Table S1** are included in supporting. This material is available free of charge via the Internet at http://pubs.acs.org.

AUTHOR INFORMATION

Corresponding Author

Shouheng Sun - Department of Chemistry, Brown University, Providence, Rhode Island 02912, United States.

Email: ssun@brown.edu.

Kotaro Sasaki - Department of Chemistry, Brookhaven National Laboratory, Upton, New York 11973, United States.
Email: ksasaki@bnl.gov

Author Contributions

S.S., K.S., H.L., K.W., and X.Z., designed/led the studies. K.W., L.P., G.H., and C.H. performed the synthesis, XRD, and ICP-AES. H.L. and K.W. studied XPS. H.L., K.W., and M.M. carried out electrochemical test. Z.Z. and G.L. completed DFT calculations. Z.H. and M.C. acquired HAADF-STEM. X.Z., N.M., and K.S. conducted *in-situ* XAS and *in-situ* IR. H.L., K.W., and X.Z. wrote the manuscript. S.S., N.M. and K.S. revised the manuscript. All authors discussed the results and reviewed the manuscript.

Notes

The authors declare no competing financial interests.

ACKNOWLEDGMENT

The work was supported in part by the US Department of Energy (DOE), Energy Efficiency and Renewable Energy, Fuel Cell Technologies Office, and by Toyota. This work used 7-BM QAS beamline of the National Synchrotron Light Source II, a U.S. DOE Office of Science User Facility operated for the DOE Office of Science by Brookhaven National Laboratory under Contract No. DE-SC0012704. Beamline operations were supported in part by the Synchrotron Catalysis Consortium under U.S. DOE, Office of Basic Energy Sciences Grant No. DE-SC0012335. Z. Z. was supported by the National Natural Science Foundation of China under grant no. 22102077, and the work at California State University Northridge was supported by the US NSF-PREM program (DMR-1828019). Microscopy was supported by DOE-BES early career award ERKCZ55, and conducted at ORNL's Center for Nanophase Materials Sciences (CNMS), which is a US-DOE, Office of Science User Facility.

REFERENCES

1. Wang, M., Han, J., Dunn, J. B., Cai, H. & Elgowainy, A. Well-to-wheels energy use and greenhouse gas emissions of ethanol from corn, sugarcane and cellulosic biomass for US use. *Environ. Res. Lett.* **7**, 045905 (2012).

2. M.A.F.Akhairia, S. K. K. Catalysts in direct ethanol fuel cell (DEFC): An overview. *Int. J. Hydrogen Energy* **41**, 4214–4228 (2016).

3. Wang, Y., Zou, S. & Cai, W.-B. Recent Advances on Electro-Oxidation of Ethanol on Pt- and Pd-Based Catalysts: From Reaction Mechanisms to Catalytic Materials. *Catalysts* **5**, 1507–1534 (2015).

4. Stanley C. S. Lai, Steven E. F. Kleijn, Fatma T. Z. Öztürk, Vivienne C. van Rees Vellinga, Jesper Koning, Paramaconi Rodriguez, M. T. M. K. Effects of electrolyte pH and composition on the ethanol electro-oxidation reaction. *Catal. Today* **154**, 92–104 (2010).

5. Kavanagh, R., Cao, X. M., Lin, W. F., Hardacre, C. & Hu, P. Origin of low CO 2 selectivity on platinum in the direct ethanol fuel cell. *Angew. Chemie - Int. Ed.* **51**, 1572–1575 (2012).

6. Weijiang Zhou, Miao Lia, Lan Zhang, S. H. C. Supported PtAu catalysts with different nano-structures for ethanol electrooxidation. *Electrochim. Acta* **123**, 233–239 (2014).

7. Lin, H. *et al.* PdAu Alloy Nanoparticles for Ethanol Oxidation in Alkaline Conditions: Enhanced Activity and C1 Pathway Selectivity. *ACS Appl. Energy Mater.* **2**, 8701–8706 (2019).

8. Kong, F. *et al.* Selective Surface Engineering of Heterogeneous Nanostructures: In Situ Unraveling of the Catalytic Mechanism on Pt–Au Catalyst. *ACS Catal.* **7**, 7923–7929 (2017).

9. Xiaoyang Fu, Chengzhang Wan, Aixin Zhang, Zipeng Zhao, Huaixun Huyan, Xiaoqing Pan, Shuaijing Du, Xiangfeng Duan, Y. H.

Pt3Ag alloy wavy nanowires as highly effective electrocatalysts for ethanol oxidation reaction. *Nano Res.* **13**, 1472–1478 (2020).

10. Vigier, F., Coutanceau, C., Hahn, F., Belgsir, E. M. & Lamy, C. On the mechanism of ethanol electro-oxidation on Pt and PtSn catalysts: electrochemical and in situ IR reflectance spectroscopy studies. *J. Electroanal. Chem.* **563**, 81–89 (2004).

11. Kowal, A. *et al.* Ternary Pt/Rh/SnO 2 electrocatalysts for oxidizing ethanol to CO 2. *Nat. Mater.* **8**, 325–330 (2009).

12. Huang, W. *et al.* Promoting Effect of Ni(OH)2 on Palladium Nanocrystals Leads to Greatly Improved Operation Durability for Electrocatalytic Ethanol Oxidation in Alkaline Solution. *Adv. Mater.* **29**, 1–8 (2017).

13. Liu, Y. *et al.* Electro-Oxidation of Ethanol Using Pt3Sn Alloy Nanoparticles. *ACS Catal.* **8**, 10931–10937 (2018).

14. Spendelow, J. S. & Wieckowski, A. Electrocatalysis of oxygen reduction and small alcohol oxidation in alkaline media. *Phys. Chem. Chem. Phys.* **9**, 2654–2675 (2007).

15. Shao, M. H. & Adzic, R. R. Electrooxidation of ethanol on a Pt electrode in acid solutions: in situ ATR-SEIRAS study. *Electrochim. Acta* **50**, 2415–2422 (2005).

16. Schmidt, V. M., Ianniello, R., Pastor, E. & González, S. Electrochemical reactivity of ethanol on porous Pt and PtRu: Oxidation/reduction reactions in 1 M HClO4. *J. Phys. Chem.* **100**, 17901–17908 (1996).

17. Huang, L., Sorte, E. G., Sun, S. G. & Tong, Y. Y. J. A straightforward implementation of in situ solution electrochemical 13C NMR spectroscopy for studying reactions on commercial electrocatalysts: Ethanol oxidation. *Chem. Commun.* **51**, 8086–8088 (2015).

18. Li, M. *et al.* Ternary electrocatalysts for oxidizing ethanol to carbon dioxide: Making Ir capable of splitting C-C bond. *J. Am. Chem. Soc.* **135**, 132–141 (2013).

19. Liang, Z. *et al.* Direct 12-Electron Oxidation of Ethanol on a Ternary Au(core)-PtIr(Shell) Electrocatalyst. *J. Am. Chem. Soc* **141**, 9629–9636 (2019).

20. Luo, L. *et al.* Composition-Graded Cu-Pd Nanospheres with Ir-Doped Surfaces on N-Doped Porous Graphene for Highly Efficient Ethanol Electro-Oxidation in Alkaline Media. *ACS Catal.* **10**, 1171–1184 (2020).

21. Wang, H.-F. & Liu, Z.-P. Comprehensive Mechanism and Structure-Sensitivity of Ethanol Oxidation on Platinum: New Transition-State Searching Method for Resolving the Complex Reaction Network. *J. Am. Chem. Soc.* **130**, 10996–11004 (2008).

22. Han, S. H., Liu, H. M., Chen, P., Jiang, J. X. & Chen, Y. Porous Trimetallic PtRhCu Cubic Nanoboxes for Ethanol Electrooxidation. *Adv. Energy Mater.* **8**, 1–10 (2018).

23. Zhu, Y., Bu, L., Shao, Q. & Huang, X. Subnanometer PtRh Nanowire with Alleviated Poisoning Effect and Enhanced C-C Bond Cleavage for Ethanol Oxidation Electrocatalysis. *ACS Catal.* **9**, 6607–6612 (2019).

24. Tarnowski, D. J. & Korzeniewski, C. Effects of surface step density on the electrochemical oxidation of ethanol to acetic acid. *J. Phys. Chem. B* **101**, 253–258 (1997).

25. M. D. Obradovića, J. R. Roganb, B. M. Babićc, A. V. Tripkovića, A. R. S. Gautamd, V. R. Radmilovićbd, S. L. G. Formic acid oxidation on Pt–Au nanoparticles: Relation between the catalyst activity and the poisoning rate. *J. Power Sources* **197**, 72–79 (2012).

26. Dingwang Yuan, Xingao Gong, and R. W. Decomposition pathways of methanol on the PtAu(111) bimetallic surface: A first-principles study. *J. Chem. Phys.* **128**, 064706 (2008).

27. Zhu, W. *et al.* Active and selective conversion of CO2 to CO on ultrathin Au nanowires. *J. Am. Chem. Soc.* **136**, 16132–16135 (2014).

28. De-Jun Chen, Y. Y. J. T. An in-situ electrochemical IR investigation of solution CO electro-oxidation on a polycrystalline Au surface in an alkaline electrolyte: Identification of active reaction intermediates. *J. Electroanal. Chem.* **800**, 39–45 (2017).

29. Sasaki, K., Marinkovic, N., Isaacs, H. S. & Adzic, R. R. Synchrotron-Based In Situ Characterization of Carbon-Supported Platinum and Platinum Monolayer Electrocatalysts. *ACS Catal.* **6**, 69–76 (2016).

30. Melke, J. *et al.* Ethanol oxidation on carbon-supported Pt, PtRu, and PtSn catalysts studied by operando X-ray absorption spectroscopy. *J. Phys. Chem. C* **114**, 5914–5925 (2010).

31. D. E. Ramaker, D. C. K. The atomic AXAFS and Dl XANES techniques as applied to heterogeneous catalysis and electrocatalysis. *Phys. Chem. Chem. Phys.* **12**, 5514–5534 (2010).

32. Arruda, T. M., Shyam, B., Ziegelbauer, J. M., Mukerjee, S. & Ramaker, D. E. Investigation into the competitive and site-specific nature of anion adsorption on Pt using in situ X-ray absorption spectroscopy. *J. Phys. Chem. C* **112**, 18087–18097 (2008).

33. Teliska, M., O'Grady, W. E. & Ramaker, D. E. Determination of O and OH adsorption sites and coverage in situ on Pt electrodes from Pt L 23 X-ray absorption spectroscopy. *J. Phys. Chem. B* **109**, 8076–8084 (2005).

34. Zhou, Z.-Y., Wang, Q., Lin, J.-L., Tian, N. & Sun, S.-G. In situ FTIR spectroscopic studies of electrooxidation of ethanol on Pd electrode in alkaline media. *Electrochim. Acta* **55**, 7995–7999 (2010).

35. Mavrikakis, M., Hammer, B. & Nørskov, J. K. Effect of strain on the reactivity of metal surfaces. *Phys. Rev. Lett.* **81**, 2819–2822 (1998).

36. Hammer, B. & Nørskov, J. K. Theoretical surface science and catalysis—calculations and concepts. *Adv. Catal.* **45**, 71–129 (2000).

37. Li, M., Liu, P. & Adzic, R. R. Platinum monolayer electrocatalysts for anodic oxidation of alcohols. *J. Phys. Chem. Lett.* **3**, 3480–3485 (2012).

38. Colmati, F. *et al.* The role of the steps in the cleavage of the C-C bond during ethanol oxidation on platinum electrodes. *Phys. Chem. Chem. Phys.* **11**, 9114–9123 (2009).

39. V. Del Colle, A. Berna, G. Tremiliosi-Filho, E. Herrero, J. M. F. Ethanol electrooxidation onto stepped surfaces modified by Ru deposition: electrochemical and spectroscopic studies. *Phys. Chem. Chem. Phys.* **10**, 3766–3773 (2008).

Table of Contents artwork